NASA DEVELOP National Program
Virginia – Langley
Spring 2021

Tonlé Sap Food Security & Agriculture

Evaluating the Effects of Land Use and Hydrological Change on Ecosystem Vitality using Remotely-Sensed Data in the Tonlé Sap Lake Basin

DEVELOP Technical Paper
Final – April 1st, 2021

Marco Vallejos (Project Lead)
Jenna Johnston
Sonnet Phelps
Joseph Scarmuzza

Advisors:
Dr. Venkataraman Lakshmi, University of Virginia, Department of Engineering Systems and the Environment (Science Advisor)
Dr. Derek Vollmer, Conservation International (Science Advisor)
Dr. Kenton Ross, NASA Langley Research Center (Science Advisor)

1. Abstract

Tonlé Sap Lake, the largest lake in Southeast Asia, is a critical source of fish and freshwater resources for the region. The health of this freshwater system is under pressure from accelerating dam construction, intensifying agriculture, deforestation, and changing climate patterns, forcing tradeoffs between immediate food security and the long-term vitality and productivity of the ecosystem. Efficient freshwater system monitoring is crucial to navigating these challenges. In collaboration with Conservation International, the Cambodian Ministry of Water Resources and Meteorology, and the Tonlé Sap Authority, we developed and tested remotely-sensed proxies for sub-indicators of the Freshwater Health Index (FHI), which is typically calculated using *in situ* datasets. We used landcover datasets derived from Landsat 5 Thematic Mapper (TM), Landsat 7 Enhanced Thematic Mapper Plus (ETM+), Landsat 8 Operational Land Imager (OLI), PROBA-V Vegetation sensor (VGT), Sentinel-2 Multispectral Imager (MSI), Advanced Very High Resolution Radiometer (AVHRR), and Envisat Medium Resolution Imaging Spectrometer (MERIS) as inputs to calculate land cover naturalness and bank modification. Additionally, we created a lake-level time series using a collection of altimetry data sources to estimate deviation from natural flow. We observed a decrease in landcover naturalness and a breakdown in the volume and regularity of annual lake levels from 2000-2020, reflecting increased pressure on water supply and agricultural productivity. At least 8% of forested areas in the basin were lost and rice harvest intensity increased over the course of the study period. These results will help our partners make informed decisions regarding freshwater management. Furthermore, our remotely-sensed FHI analysis can be replicated in other regions, providing decision makers with a snapshot of freshwater health in data-scarce environments.

Key Terms

Freshwater Health Index, conservation, inland water body, remote sensing, land use/landcover, lake level change, altimetry, irrigation, Google Earth Engine

2. Introduction

2.1 Background Information

The Tonlé Sap Lake and River Basin is a unique hydrological system that has allowed civilizations to flourish in the area for millennia. Home to more than 4.5 million people, with nearly a million living directly on the lake in floating villages, this densely populated biodiversity hotspot “is of international significance culturally, hydrologically, and ecologically” (Campbell et al. 2009). The Mekong River’s flow reversal causes the lake to increase in surface area from 3,000 to more than 15,000 square kilometers during the monsoon season each year (Figure 1) (Uk et al. 2018). This flood pulse deposits nutrient-rich silt onto floodplains used for rice cropping and allows for fish to spawn in protective habitats. Rice and fish from the lake basin fulfill 40% of the protein needs of the entire population of Cambodia (D. Vollmer, personal communication).

Figure 1. Map of the Tonlé Sap Lake Basin, with dry season lake extent and monsoon season lake extents visualized on the lake.

Over the past decades, following Cambodia's post-occupation recovery, significant shifts in the country's economic and political landscapes have resulted in an expansion of the export economy. However, the accelerating use of vast ecological resources has burdened the nation's vulnerable and future populations (Ingalls et al. 2018). Forest cover within the Tonlé Sap Lake Basin has declined due to logging and agricultural expansion by 43% from 1990 to 2009, the fastest deforestation rate in Cambodia (Uk et al. 2018). Recently, dams on the Mekong and its tributaries upstream of Cambodia have been under construction to supply surrounding nations with hydroelectric power. Studies such as Lin & Qi (2017) and Arias et al. (2014a, 2014b) have demonstrated the extreme and destructive effects of the resulting hydrological changes.

Our study spans the years 2000 to 2020, a period of rapid regional change in landcover and hydrology. Global- and regional-scale shifts in precipitation and seasonality make flood pulses more unpredictable, which harms agricultural systems, natural vegetation, and infrastructure near the floodplain border (Nuorteva et al. 2010). Hotter dry seasons are also worsening damage related to fires in flooded forests, which are sometimes set intentionally for agricultural purposes, but can spread and damage habitats not adapted to a fire regime (Mahood et al. 2020). A deteriorating ecological system within Tonlé Sap Lake Basin threatens biological diversity and productivity.

This project is scientifically rooted in Conservation International (CI)'s Freshwater Health Index (FHI), which was designed to close the information gap between ecosystem health and impacts on livelihoods (Vollmer et al. 2018). The FHI, a conceptual framework and a piece of Windows software, summarizes data into three indicators scaled from 0-100: ecosystem vitality, ecosystem services, and

governance (Vollmer et al. 2018). The FHI is currently configured to integrate a variety of data types, emphasizing *in situ* data and stakeholder input. This process can be time-consuming and resource-intensive, especially in data-scarce regions, and while facing pandemic-related barriers to international work (Conservation International 2018). Due to the challenges of *in situ* data collection, we tested the feasibility of using remote sensing to evaluate freshwater system health. Earth observations (EOs) have been used to derive land use and landcover globally (Gong et al. 2013) and regionally in Southeast Asia (Spruce et al. 2018, Poortinga et al. 2019, Saah et al. 2019a, Saah et al. 2019b). Analyzing lake level fluctuation using altimetry is helpful in areas where *in situ* lake level measurements are scarce (Gottl et al. 2016, Hossain et al. 2017, Chang et al. 2019).

2.2 Project Partners & Objectives

The project was conducted in collaboration with Conservation International (CI), an international organization that works to conserve ecosystem services in order to support sustainable livelihoods and local economies. They have worked directly in the Tonlé Sap Lake region since 2001 to support freshwater ecosystem health and promote sustainable livelihoods (D. Vollmer, personal communication). CI will use our results to inform ongoing collaboration with regional organizations, including Cambodia's Ministry of Water Resources and Meteorology (MoWRaM) and the Tonlé Sap Authority (TSA), to support decision-making and water resource management. The Asian Development Bank and the World Bank are additional collaborators interested in how findings may relate to efforts they fund in the region.

The focus of this project was to identify and prototype remotely-sensed inputs for FHI sub-indicators in the Tonlé Sap Lake region. We chose to investigate landcover naturalness and bank modification from the drainage basin condition indicator, as well as the deviation from the natural flow sub-indicator as part of water quantity. Inputs into the FHI for the Tonlé Sap Lake Basin included landcover naturalness from 2000-2020, derived from various classification datasets, as well as a calibrated lake level time series derived from satellite altimetry. In addition to investigating ecosystem changes specific to Tonlé Sap Lake Basin, scientists at CI tasked our team with designing an application for FHI analysis in Google Earth Engine (GEE), in order to conduct faster estimates of baseline freshwater system health using remotely-sensed data in other watersheds with varying levels of *in situ* data availability.

3. Methodology

3.1 Sub-indicator selection

Some FHI indicators, such as most aspects of Governance & Stakeholders, are impractical to evaluate using EOs. The ecosystem vitality indicator is environmentally oriented and quantitatively measurable, so its sub-indicators are well disposed to EO applications. For drainage basin condition, the FHI measures landcover naturalness (LCN), which is a standardized metric of land cover classes' hydrological impacts averaged across the watershed. Bank modification (BM) is a similar metric of average naturalness, which places a higher weight on areas that have a more direct impact on watershed health by isolating areas 100 meters or less from permanent water features.

3.2 Lake Level Altimetry

3.2.1 Data Acquisition

To develop a lake-level time series, we used altimetry data from the Database for Hydrological Time Series of Inland Waters (DAHITI), developed by researchers at the Technical University of Munich. This tool aggregates altimetry data from a number of global satellites, including TOPEX-Poseidon, the Jason series, Envisat, and SARAL-AltiKa, aggregating over a central node in each inland water body (Schwatke et al. 2015). SERVIR-Mekong has also developed a similar tool called AltEx (Markert et al. 2019), but it is still in development. DAHITI offers the most complete temporal coverage we could find, as it pulls from a number of satellites with different paths across Tonlé Sap Lake. The full list of satellites used in the DAHITI dataset is given in Table A1, and an image of a number of these altimetry tracks, along with the nodes at which DAHITI aggregates altimetry data, is given in Figure A1.

To validate the altimetry measurements against *in situ* data, we also sourced river gauge data from our partners at CI. They provided data from four river gauges dating back to the 1960s, which was useful for developing a model of historical flow. The locations of the river gauges are indicated by the yellow markers in Figure A2. We mapped them on top of HydroSHEDS DEM to indicate their elevation relative to the lake's surface. The elevation of the Kampong Thmar, Prek Kdam, and Phnom Penh Port river gauges are 15m, 10m, and 18m above sea level, respectively.

3.2.2 Data Processing

The altimetry data we downloaded from DAHITI was substantially pre-processed. In addition to outlier filtering and orbital height correction, Schwatke et al. (2015) aggregated values from multiple altimetry missions using a Kalman filtering algorithm. This processing is valuable because it enables the use of various altimeters and eliminates the need for heavy processing of raw altimetry data. In order to eliminate constant offsets between river gauge and altimetry time series and render them comparable to one another, we also needed to shift the altimetry time series to the level of the *in situ* data such that changes in water level are not obscured by a regular offset (Schwatke et al. 2015). To do so, we filtered both datasets to include only days for which data from both sources were available. Then we calculated the mean height difference between these two time series to estimate the constant offset between them and subtracted this estimated offset value from each value in the altimetry data to yield a corrected time series.

3.2.3 Data Analysis

To calculate the Deviation from Natural Flow FHI sub-indicator, we needed to replicate the calculations described in the FHI documentation. To quantify the impact of anthropogenic regulation on water supply, the FHI calculates the deviation between a modeled "unregulated" and an actual "regulated" timeseries and then assigns a weighted naturalness score. For the first step, we followed CI in using the formula for Amended Annual Proportion of Flow Deviation (AAPFD; Equation 1), derived from Gehrke et al. (1995), where m_i is "monthly flow data accruing to current condition" and n_i is "modeled natural flow for the same period" (Vollmer et al. 2018).

$$AAPFD = \sum_{j=1}^{p} \frac{\sqrt[2]{\sum_{i=1}^{12} \left[\frac{m_i - n_i}{\overline{n_i}}\right]^2}}{p}$$

(1)

We used a simple model of monthly averages from historical river gauge data to estimate "unregulated" flow for n_i in the formula above. We selected the time period of 1960-1990 for this historical baseline, both because reliable river gauge data became available starting in 1960 and because no large dams existed in the Mekong River basin prior to 1990 (N. Souter, personal communication). Comparing current altimetry data to this historical baseline thus simulates comparison between present-day flow, regulated by dams, irrigation, and other human interventions, and what flow might look like without those interventions.

Because calculating AAPFD for a single year of current altimetry data against thirty-year average risks can generate erroneous deviation scores (N. Souter, personal communication), we calculated rolling five-year monthly averages from the altimetry timeseries from 2007 (a cumulative average starting in 2002, the first year of our altimetry timeseries) to 2020 and outputted an AAPFD value for each of these years (see Appendix A). We subsequently applied CI's scoring schema to assign each AAPFD value an Ecosystem Health Score (EHS) ranging from 0 to 100, where 100 represents no deviation from the natural flow regime (N. Souter, personal communication). Higher AAPFD values indicate more deviation and thus receive a lower EHS score. These EHS scores form the inputs for the overall FHI calculation.

We performed all of these calculations in a Python script and created a reusable function that can intake current altimetry data and output its deviation from the historical average flood pulse. This will allow end users to quickly input the lake levels from a given year and determine the current level of stress on the water supply. This code could be incorporated into future iterations of the comprehensive FHI tool.

3.3 Land Use and Land Cover

3.3.1 Data Acquisition

We loaded four landcover datasets into Google Earth Engine (GEE) for naturalness assessment. The two global landcover datasets we utilized were the European Space Agency (ESA)'s Copernicus Global Land Cover System (or CGLS, 100m resolution, annual 2015-2019), and ESA's Climate Change Initiative land cover (or CCI, 300m resolution, annual 1992-2015). CGLS maps were summoned from the GEE data catalog, and CCI maps were downloaded from their website and uploaded into GEE as assets. We also used SERVIR-Mekong's Regional Land Cover Monitoring System (RLCMS), which has annual landcover maps and landcover class primitives available at 30m resolution from 2000-2018 and was accessed directly in GEE using SERVIR's file pathnames. Finally, we uploaded an official Cambodian Ministry of Energy (MoE) landcover map from 2016 provided by our partners, which utilized the Food and Agriculture Organization's methodology, into GEE. The EOs that each of these datasets is based on is available in Table B1.

Global datasets provide inputs to naturalness on a global, albeit less accurate, scale. This is useful for easy replicability in other study sites. The national MoE map demonstrates the possibility of integration with existing, preferred governmental data systems. SERVIR-Mekong's regional maps receive an overall accuracy of almost 95% and are accompanied by input layers of probability for each class, called primitives, which assemble training data from a multitude of variables for each year. The RLCMS, therefore, provided the basis for constructing a hydrology-oriented Tonle Sap Basin classification.

Datasets for other indices available in GEE were used as end-members to separate classes with divergent hydrological impacts, producing more realistic FHI scores through greater specificity. These end members were called directly from GEE servers and include NASA's Shuttle Radar Topography Mission Digital Elevation Model (STRM DEM, elevation in 2000 at 30m resolution), NASA's Landsat 8 OLI imagery (for indices since 2013, 30m resolution), Terra and Aqua Moderate Resolution Imaging Spectroradiometer (MODIS, for indices, since 2000 and 2002 respectively, 250m resolution), and Visible Infrared Imaging Radiometer Suite (Normalized Difference Vegetation Index [NDVI], 2012-2020, 500m resolution).

3.3.2 Data Processing

We utilized these landcover datasets to output two drainage basin condition sub-indicators: land cover naturalness (LCN) and bank modification (BM). We clipped each landcover dataset to the Tonlé Sap Lake watershed for LCN analyses. For BM, we performed an additional clip, including pixels within 100 meters of permanent surface water features within the watershed.

We consulted with partners at CI to determine how to convert categorical landcover classes to naturalness values scaled from 0-100. These naturalness scores were based on the FHI's existing weighting scheme (Vollmer et al. 2018) and CI's knowledge of ecology and land use change in the basin. Other locations should use different weighting schematics based on local ecology. After computing the percentage of pixels representing each class across the basin, we exported these statistics (land cover naturalness and bank modification) calculated for each year that each dataset was available.

In order to get a baseline understanding of forest loss, we wrote a function that outputted the overlay between pixels classified as forest in the first year of the dataset and those classified as non-forest in the last year of the dataset. We then divided the count of forest loss pixels by a count of original forested pixels to estimate the percentage of forested area lost over the study period. We produced a naturalness output with deforested areas reweighted with a lower naturalness value, which was very similar to the original output.

Rice crops in the Tonlé Sap area are usually harvested once annually during wet-season flooding, but some paddies now use irrigation and fertilizers to harvest rice two or three times per year. Using the ancillary end-members we assembled in GEE, we tested the feasibility of separating rice areas according to harvest frequency by comparing indices during each harvest month. In order to discern which indices can be used to identify differences in rice areas, we used NDVI from Landsat, VIIRS, and Terra & Aqua MODIS; NDWI from Landsat and Terra & Aqua MODIS; surface temperature from Landsat and Terra & Aqua MODIS; elevation

from the NASA STRM; EVI from VIIRS; and Synthetic Aperture Radar data from ESA's Sentinel-1 series. We derived threshold values for each index in each harvest month from corresponding harvest frequency classes in an existing rice mapping effort focused around the Vietnamese Mekong Delta (V. Lakshmi, personal communication). These thresholds, applied to SERVIR-Mekong's RLCMS yearly map rice masks, separated rice pixels into single-, double-, and triple-harvest classes.

3.3.3 Data Analysis
In order to compare classifications, we visualized each in GEE. We leveraged our conversions to standardized naturalness to find the simple arithmetic difference between naturalness for corresponding pixels across different classification algorithms. Difference maps between each pair of classifications for 2015 (2016 for MoE's map) were produced, as well as a variance map indicating the degree of disparity in naturalness determinations for each pixel. Some comparisons showed greater disagreement than others, especially in particular classes. We created an overall variance map and lastly correlated the output scores to quantify agreement between classifications.

We used primitives, or single-class input layers, from the SERVIR dataset to filter for high-probability locations independently, and used a stratified sample of class points to assess the accuracy of each class in the final RLCMS map. We constructed an error matrix to derive producer's and consumer's accuracy of each class and used these accuracies to adjust the proportions of each landcover class. Then we exported adjusted percentage area by class, LCN, and BM outputs to compare with our non-error-adjusted outputs.

4. Results & Discussion

4.1 Results

4.1.1 Lake Level
After performing the correction step described in section 3.2.1 to adjust the altimetry data to the water level of each river gauge and render the datasets more readily comparable, we visually assessed the correlation between the altimetry time series and each river gauge time series by plotting them on the same axes (Figure 2). Spearman correlation tests between altimetry and each river gauge time series indicated a very strong relationship between altimetry and gauge data (Kampong Thmar: $r = 0.808$, $p < 2.2 \times 10^{-16}$; Prek Kdam: $r = 0.953$, $p < 2.2 \times 10^{-16}$; Phnom Penh Port: $r = 0.923$, $p < 2.2 \times 10^{-16}$; Kampong Luong: $r = 0.984$, $p < 2.2 \times 10^{-16}$). To examine their relationships more closely, we also plotted the remaining differences between the two datasets, calculated for days on which both data sources were available, in the subplots below (Figure 2). The periodic pattern visible in these residual plots is attributable to the predictable temporal offset between changes in lake height and changes in the heights of the tributaries where the gauges are located.

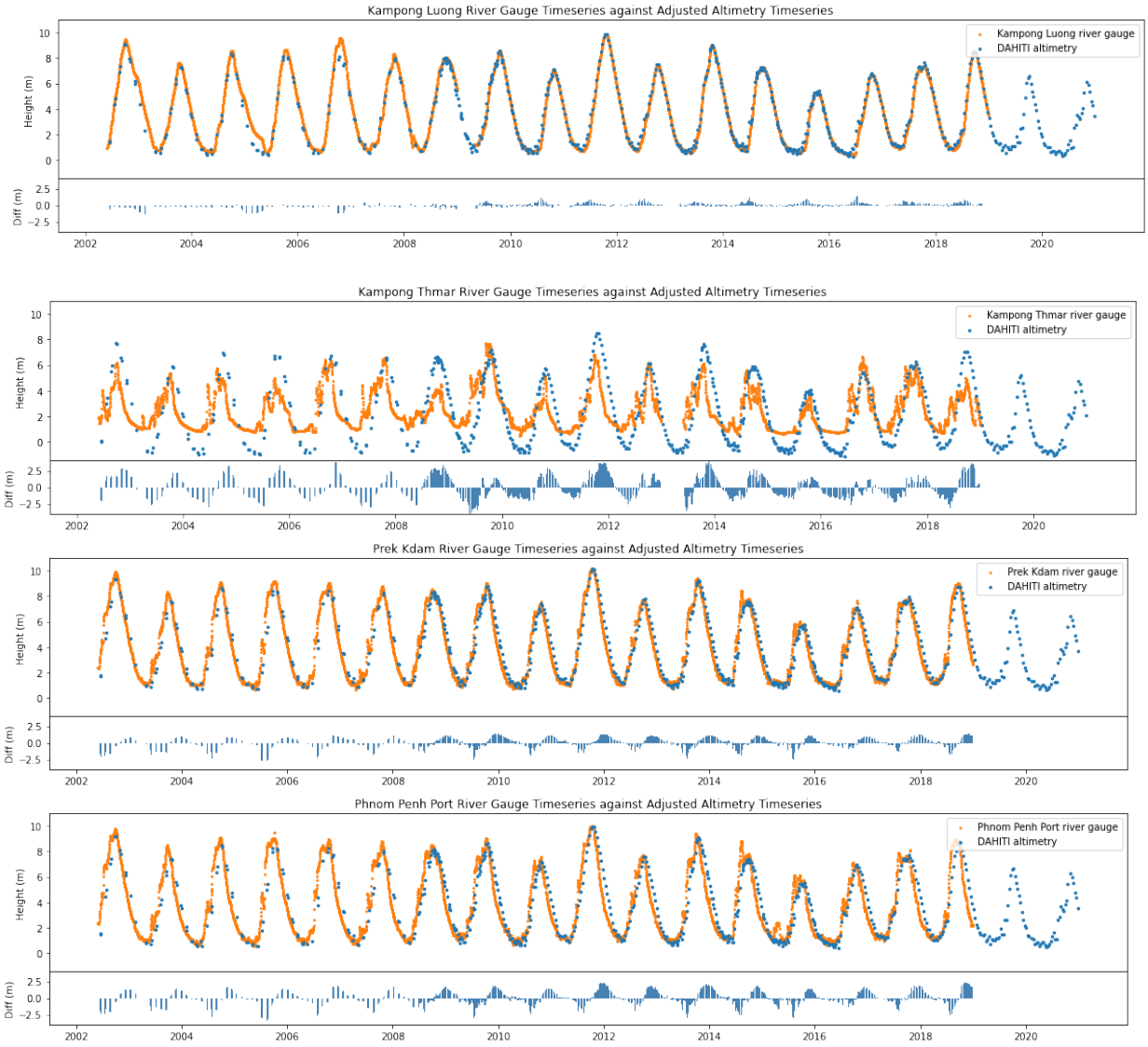

Figure 2. Water level time series for the center of Tonlé Sap Lake from DAHITI, shifted to the water level height of the *in situ* river gauge data, plotted (in orange) against each of the river gauge time series provided by CI (in blue) for days on which both data sources are available. The remaining differences in height between altimetry and river gauge data are plotted in the lower subplots.

The rationale for this comparison was twofold. First, we wanted to validate the use of altimetry data as a proxy for *in situ* water height, for which CI typically uses river gauge data, in the context of generating an FHI for a large freshwater lake.

The close visual alignment and high correlation scores between the DAHITI altimetry data and the river gauge time series suggest that altimetry is indeed a useful proxy. Second, we wanted to determine which river gauge datasets would be most reliable for use in our model of the historical baseline.

Because we observed significant variability and a relatively low correlation score in our comparison of the altimetry time series to the Kampong Thmar river gauge data, we decided to eliminate that river gauge dataset from our DvNF (deviation from natural flow) calculations. We also observed a subtle positive trend in the residuals from the comparison between the altimetry time series and the Kampong Luong river gauge data, which suggests an ongoing directional shift in the heights detected by the Kampong Luong river gauge (as we did not observe such a trend in any of the other comparisons with the same altimetry data). Because we could not determine whether this trend is related to a natural phenomenon or is an artifact of the river gauge technology, we chose also to eliminate the Kampong Luong time series from our DvNF calculations. Furthermore, the Phnom Penh Port and Prek Kdam river gauges had the most continuous time series durations, starting in 1960 and continuing to 2018, while the Kampong Thmar gauge data had a gap from around 1970 to 1983, and Kampong Luong a gap from 1965 to around 1995. For these reasons, we elected to average the river heights from just the Phnom Penh Port and Prek Kdam gauges, which had a strong correlation with the altimetry data and a pattern of residuals attributable to natural flow phenomena in the years 2002-2018, for use in the historical baseline model.

To compare the current altimetry time series with the historical baseline model we calculated, we plotted the altimetry data for each year over a curve with a width of +/- 1 standard deviation of the monthly historical averages (Appendix A). While the first eight years of the study period remain more or less within range of the historical baseline, we observe increasing deviation from the baseline in the more recent portion of the study period. In the years 2010-2013, as well as in 2016, 2019, and 2020, we observe a delay in the occurrence of the wet-season water height peak, which is consistent with literature describing delays in the annual flood pulse (Uk et al. 2018, Arias et al. 2014a, Arias et al. 2014b). We observe the most dramatic deviation from the historical baseline in the years 2015, 2019, and 2020. Aggregating the information presented in Figure A3 into a summary plot of the first six and last six years of the study period (Figure 3) makes the recent breakdown in regularity and overall height of annual lake levels readily apparent.

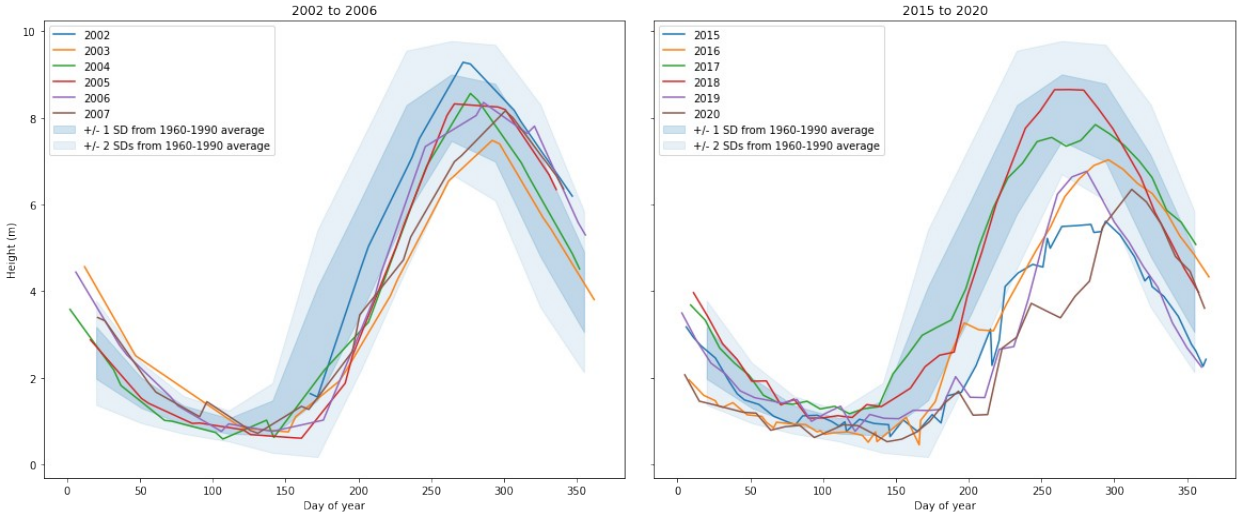

Figure 3. Altimetry data for the first six and last six years of the study period (colors correspond to years indicated in plot legend) plotted over +/- 1 (darker blue) and +/-2 (lighter blue) standard deviations from the historical baseline.

We recognize that significant changes in hydrology could also partly result from environmental factors on a broader regional scale, which may be confounding to the local, anthropogenic variables being investigated. We performed correlation tests against potentially confounding environmental variables including precipitation, evaporation, and drought and the DvNF scores generated from the rolling 5-year averages of the altimetry data against the historical baseline and did not discover any major correlations, suggesting that the observed changes in lake level are likely attributable to human intervention rather than confounding environmental variables. In our contextual research, upstream dam construction and mounting pressure on the water supply to irrigate intensifying agriculture emerged as the two biggest anthropogenic drivers of water level fluctuations (Arias et al. 2014a, Arias et al. 2014b).

4.1.2 Land Cover

We calculated LCN and BM using four annual landcover datasets, including two global datasets (CCI, 300-meter resolution, 2000-2015; and Copernicus, 100-meter resolution, 2015-2019), one regional dataset (SERVIR RLCMS, 30m resolution, 2000-2018), and one national dataset (Cambodian Ministry of Energy [MoE] map, 30m resolution, 2016). For the entire basin, LCN and BM scored in the 50s and 60s out of 100 (Figure 4) (Figure B2). We also scored each sub-basin separately, which varied from 40 near large cities like Phnom Penh, to nearly 70 in other regions (Figure B3). Scores derived from the error-adjusted versions of RLCMS class proportions were slightly lower and declined at a faster rate (Figure B4).

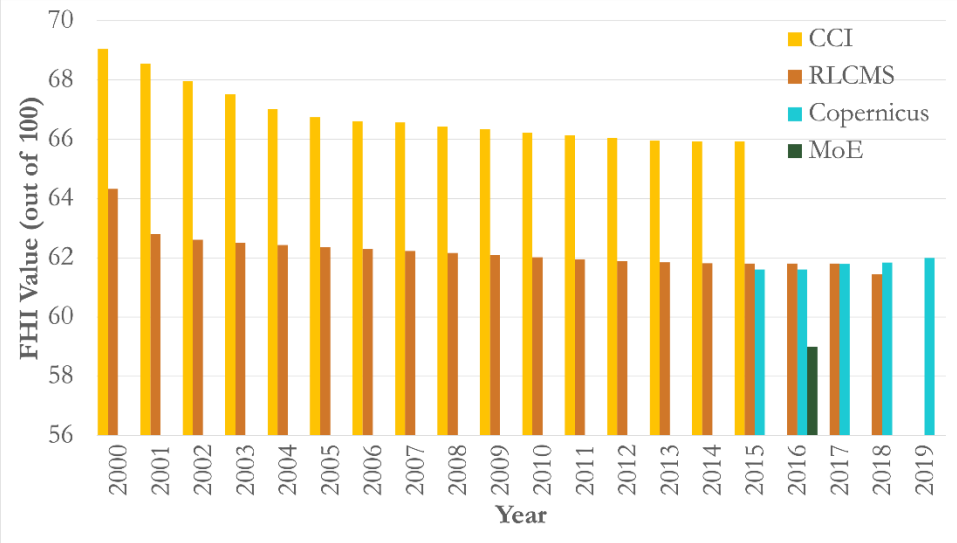

Figure 4. Land cover naturalness output values out of 100 for the 4 land cover datasets: CCI, RLCMS, Copernicus, and Cambodian MoE. Each dataset is represented for all the years in which that dataset is available.

Difference maps show clear patterns between typologies; variance across the maps reveals that particular classes show greater variability in naturalness appraisals (Figure B5). The orchard/plantation class comprised over 40% of all high-variation locations (over 10% variance), while cropland and wetland each represented about 18% and mixed forest was 15%. CCI had higher LCN outputs than other datasets. This was likely due to the ways each landcover dataset classified agriculture. CCI separated agriculture into rainfed and irrigated agriculture, while other classifications did not make this distinction. The FHI scores rainfed agriculture as 40/100 and irrigated agriculture at 30/100. For the datasets that did not distinguish between rainfed and irrigated agriculture, we took the average of these weights and scored all agricultural areas at 35/100. This suggests less than half of agriculture is actually irrigated. We used CCI's existing classes to score rainfed and irrigated agriculture differently, and the majority of agricultural pixels for CCI in our watershed were rainfed agriculture pixels that scored 40, which contributed to CCI scoring higher for LCN than other datasets.

For BM, we calculated the score based on the naturalness of the land within 100 meters of permanent water features, placing a higher overall weight on areas that have a more direct impact on watershed health. These values ranged from 62 to 59 for SERVIR and were lower than LCN values across all datasets (Figure B2), indicating higher land change in areas that directly impact water bodies. BM similarly varied across sub-basins.

According to Pearson’s product-moment correlations, CCI and RLCMS LCN outputs were strongly positively correlated at 0.905 ($p < 1.5 \times 10^{-6}$). Within RLCMS, LCN and BM were strongly correlated at 0.995 ($p < 2.2 \times 10^{-16}$). This confirmed that LCN outputs across datasets were similar and comparable to each other, even though the original landcover classifications were based on different satellite data, training datasets, and methodology. Additionally, RLCMS LCN negatively correlated with year ($r = -0.819$, $p = 1.8 \times 10^{-5}$), as did CCI LCN (r = -

0.916, $p = 6.1 \times 10^{-7}$), demonstrating that in Tonlé Sap Basin, as year increases, land cover naturalness goes down.

We also used landcover to detect forest loss. Copernicus data showed a 1.1% loss in forest area from 2015-19. CCI and SERVIR showed that 8-9% of the basin's forests were lost over the study period, a high deforestation rate. According to the Hansen Global Forest Loss dataset, the amount of forest actually lost in the basin in this period is around 15%. This difference is related to the fact that we noticed some anomalies in the early years of SERVIR, which was likely a misclassification due to lack of training data. It is difficult to distinguish flooded forest from other wetlands using Earth observations on a regional scale due to the complex interactions between tree canopy and surface water. This did not impact our overall scores, however, because these similar classes have the same LCN weight of 100.

Incorporation of harvest frequency into the naturalness weighting schematic would make FHI scores more realistic. According to SERVIR, total rice area peaked around 2009 at about 2.25% of the basin. The amount and proportion of single-harvest rice decreased gradually from around 95% of rice area to around 35% from 2000-2018. Meanwhile, the proportion and amount of double-harvest crop fluctuated but generally trended upwards from 4% to 22%, and triple-harvest paddies increased throughout the period from under 5% to 44% in 2018, eclipsing single rice (Figure B6). These changes observed in rice agriculture are difficult to validate but align with insights from local experts.

The adjusted scores and proportions portrayed trends, which are more reflective of background literature on landscape change in the basin, with the greatest decline in naturalness occurring between 2012 and 2013 (Figure B4). Our methods for evaluating deforestation and rice intensity proved feasible for derivation from existing classifications, but the degree of accuracy of these products is difficult to assess in the absence of robust training data, so we used background information to verify these products.

4.2 Discussion

4.2.1 Feasibility

Remote sensing offers great improvements in the availability of data over spatial and temporal scales and makes the process of monitoring freshwater health faster and less resource-intensive. The remotely sensed FHI proxies we calculated in this work were comparable to values derived from *in situ* data. Specifically, we found that aggregated global altimetry data provides a meaningful proxy for *in situ* water height measurements and enables long-term monitoring of water level behavior. Work remains to distinguish human demands on lake water from climactic changes in weather patterns as the cause of diminishing water levels. Additionally, performing land cover classification with satellite imagery affords a significant advantage over conducting land surveys in the field, but is dependent on the availability and quantity of training and reference data, as well as the quality of imagery. New, freshwater health-oriented, ecosystem-specific land cover classes were difficult to validate in this case but an effort's degrees of specificity and accuracy can be improved based on the user's resources and requirements.

4.2.2 Global FHI Tool

We started the development of a Google Earth Engine tool that will enable researchers to derive a baseline FHI using remotely sensed data in any region around the world. This currently includes Copernicus and CCI global landcover products, and may eventually incorporate global altimetry available from DAHITI. This term, we were able to complete code in GEE that outputs LCN and BM statistics for anywhere in the world. It allows the user to specify a desired watershed by clicking on a location and designating a basin hierarchy level. Naturalness weights can be customized based on the specifics of local ecology. It also includes a function that can detect change from one landcover class or group of classes to another over any timestep within any typology. The user can also easily import additional local or regional landcover datasets and get more accurate LCN and BM outputs by updating dictionaries within the code to reflect these datasets' typologies, as has been accomplished for the Tonle Sap Basin. We expect that next term, this tool will be refined and updated to incorporate other FHI inputs so that it can be handed off to CI and other interested partners.

4.3 Challenges and Limitations

The present study is limited to the Tonlé Sap Lake watershed over the years 2000-2020, with various products limited by data availability and accuracy. The global datasets we used for landcover mapping have limited accuracy on the local level, in part due to tropical cloud cover preventing consistent availability of clear satellite imagery. As such, training data is limited in tropical environments, making it difficult to detect locally-specific classes at this scale. Furthermore, land cover products tend to exhibit low year-to-year reliability of land cover products, as accuracies decline unless training data collection is maintained and classification typology is updated. Additionally, surface water dynamics around TSL make land cover change difficult to assess in cases with tree canopy cover.

Although the DAHITI altimetry data was rigorously processed, altimetry faces inherent limitations when used in the context of inland water bodies. Because radar altimetry was designed to measure ocean height, it is prone to contamination by surrounding land as well as lake-specific hydrodynamic effects of wind and waves. Our present study assumes a uniform surface across the lake; future work could incorporate more detailed bathymetry and hydrology to account for differences across the lake's 16,000 km^2 surface. Furthermore, our approach of applying a uniform correction to align the altimetry data to the river gauge height is prone to systematic error.

For these reasons, the sub-indicators derived from Earth observations must be considered along with their respective margins of error. Although corrections for imagery, as well as for altimetry water-level readings, have improved the ability to rely on remote sensing data, it should be considered a complement to, rather than a replacement for ground-truthed data. In future efforts to develop the complete set of FHI sub-indicators, a number of the indicators, especially in the Governance and Ecosystem Services, will require data that is impossible to sense remotely. A hybrid model that integrates remote sensing with locally sourced data will be necessary to provide a complete picture of the health of a given freshwater system.

Furthermore, our communication with local partners was limited due to pandemic-related barriers and our project's time constraints. Although we bring remote sensing expertise, we lack a deep understanding of community concerns. Although

we designed our methods and outputs in close partnership with CI who work closely with organizations local to the Tonlé Sap Basin, we did not receive direct input from local stakeholders and thus cannot be sure that they are aligned with local freshwater health management strategies.

4.4 Future Work

There are many possible avenues for validation and extension of the work we have done this term. The next DEVELOP team will have the opportunity to continue refining our examination of land cover and land use change, including developing methods to assess change persistence and tuning rice classification and forest clearance detection. We anticipate that the next team will also explore the potential of EOs to approximate additional FHI sub-indicators. For the groundwater storage sub-indicator of water quantity, the Gravity Recovery and Climate Experiment (GRACE), launched in collaboration with the National Aeronautics and Space Administration (NASA) in 2018, can use gravity anomaly detection to understand the distribution of groundwater mass around the globe (Pham-Duc et al., 2019). For water quality, indices such as total suspended sediment, nutrients, and pollutants in bodies of water could be derived from satellite imagery (Ross et al. 2019, Wang et al. 2020). Global datasets of river networks can be used to study flow connectivity, but a dataset of dams or method for classifying dams from imagery is necessary for a realistic portrayal. Additionally, recent efforts have begun to derive estimates of relative biodiversity from related remote sensing variables such as vegetation structural diversity, temperature, and rainfall to approximate biodiversity at a regional or global scale (Schüßler et al. 2020, Pettorelli et al. 2014). While the ecosystem services, governance, and stakeholders indicators are less amenable to remote sensing, a data framework could reference spatialized datasets of economic or demographic to integrate these with remotely-sensed indicators. The team will also take time to make the GEE tool more flexible and user-friendly to allow for the incorporation of *in situ* data where available and to increase its usefulness for CI and other international NGOs.

Beyond the two terms of this project, improvements in lake-related remote sensing technology and data availability provide new directions for research. NASA's SWOT (Surface Water and Ocean Topography) satellite will launch in February 2022 and will provide high spatial and temporal resolution measurements of freshwater bodies across the world (K. Ross, personal communication). Another intriguing direction for research that will become more feasible as global datasets become available at higher spatial resolution would be to investigate freshwater health as it varies within the lake itself using lake bathymetry and shoreline variation.

We also believe there is room for additional tuning of the FHI scoring schema to be more sensitive to remotely-sensed observations. Based on the scientific literature, discussions with science advisors, and a review of local media, we understand that the Tonlé Sap Basin has undergone dramatic hydrologic changes in the past 20 years. The ecosystem has been in a state of ongoing degradation due to dams, climate change, and intense deforestation (Uk et al. 2018). Although many of our remotely-sensed data exhibits evidence of these changes – evident delays in annual wet season lake volume peaks in altimetry data or intensification of rice agriculture based on harvest frequency, for instance – the EHS scores we

calculated for the DvNF and LCN/BM outputs using the FHI's weighting schema did not reflect the dramatic downward trend over the past 20 years that our background research would suggest. In other words, the methods by which the FHI currently summarizes detailed insights derived from satellite data products into EHS scores may not be sensitive to all the types of change that we are observing, and future researchers could explore avenues to account differently for them.

5. Conclusions

The health of the Tonlé Sap Lake Basin is critical to food security and livelihoods in Cambodia and the surrounding region. Resource constraints and regional environmental change have exacerbated the tension between the need to preserve ecosystem health by maintaining fisheries and supporting biodiversity, and the need to develop irrigation infrastructure to support economic development and food security. To negotiate this balance, efficient and reliable mechanisms for assessing the status of specific freshwater health indicators are necessary.

Our investigation of the potential of remote sensing in Conservation International's FHI has demonstrated that radar altimetry and high-resolution land use and land cover mapping are useful proxies for *in situ* measurements. We observe that the Tonlé Sap watershed is experiencing declines in water quality and flood pattern regularity. Land cover naturalness is also declining due to agricultural expansion. For 2018, the region receives a combined Ecosystem Vitality score of 59/100, which reflects substantial ecosystem degradation since the early 2000s. The remotely-sensed values we calculated were comparable to values derived from *in situ* data, showing that remote sensing is an effective way to make baseline freshwater health monitoring faster and less resource-intensive. These FHI scores, however, provide only a coarse snapshot of the detailed insights on the advantages of remote sensing in freshwater health assessment in the Tonlé Sap Basin. Because the Tonlé Sap Authority and MoWRaM's expertise are based primarily on *in situ* data collection, management, and dissemination, providing them with remotely-sensed analyses over the last few decades will facilitate decision-making around development and conservation in this region.

6. Acknowledgments

We'd like to extend our gratitude to Professor Venkataraman Lakshmi and his lab at the University of Virginia, including his graduate students Manh-Hung Le and Chelsea Dandridge for their guidance. We're also grateful to our partners and advisors at Conservation International, in particular Dr. Derek Vollmer for his consistent support and FHI expertise, Dr. Nicholas Souter for his insights specific to the Tonlé Sap Region, and Max Wright for his remote sensing expertise. Additionally, we'd like to thank Kel Markert and Amanda Markert of the NASA SERVIR Science Coordination Office. Finally, we are grateful to our LaRC fellow, Adriana Le Compte, for ongoing support and feedback, and to Dr. Kenton Ross, our Langley science advisor, for his consistent support and valuable input on methodologies and project scope.

This material contains modified Copernicus Sentinel data (2015-2019), processed by ESA.

Any opinions, findings, and conclusions or recommendations expressed in this material are those of the author(s) and do not necessarily reflect the views of the National Aeronautics and Space Administration.

This material is based upon work supported by NASA through contract NNL16AA05C.

7. Glossary

Earth observations (EOs): Satellites and sensors that collect information about the Earth's physical, chemical, and biological systems over space and time
DvFN: Deviation from natural flow of water in rivers surrounding the basin
Freshwater Health Index (FHI): Conservation International's tool for connecting ecosystem vitality to ecosystem services and governance
Google Earth Engine: Powerful, cloud-based, open-source platform for geospatial analyses, hosting datasets for easy visualization and manipulation of raster data in a code editor.
Radar altimetry: Sensor that measures time taken for a radar pulse to travel from the satellite antenna to the satellite receiver
MODIS: Moderate resolution Imaging Spectroradiometer
MoWRaM: Cambodia Ministry of Water Resources and Meteorology
SAR: Synthetic Aperture Radar
SERVIR: A joint NASA and USAID operation that works with developing countries to utilize NASA Earth observations
TSA: Tonlé Sap Authority (Cambodian government ministry)
SWAT: Soil and Water Assessment Tool, a water quality modeling tool
SWOT: Surface Water and Ocean Topography, a surface water satellite launching in February 2022

8. References

Arias, M. E., Piman, T., Lauri, H., Cochrane, T. A., & Kummu, M. (2014a). Dams on Mekong tributaries as significant contributors of hydrological alterations to the Tonle Sap Floodplain in Cambodia. *Hydrology and Earth System Sciences*, *18*(12), 5303–5315. https://doi.org/10.5194/hess-18-5303-2014

Arias, Mauricio E, Cochrane, T. A., Kummu, M., Lauri, H., Holtgrieve, G. W., Koponen, J., & Piman, T. (2014b). Impacts of hydropower and climate change on drivers of ecological productivity of Southeast Asia's most important wetland. *Ecological Modelling*, *272*, 252–263. https://doi.org/https://doi.org/10.1016/j.ecolmodel.2013.10.015

Buchhorn, M., Smets, B., Bertels, L., De Roo, B., Lesiv, M., Tsendbazar, N.E., Linlin, L., & Tarko, A. (2020). *Copernicus Global Land Service: Land Cover 100m* (Version 3, Global 2015-2019) Zenodo, Geneva, Switzerland, https://doi.org/10.5281/zenodo.3938963

Campbell, I. C., Say, S., & Beardall, J. (2009). Tonle Sap Lake, the Heart of the Lower Mekong. In Ian C. Campbell (Ed.), *The Mekong: Biophysical environment of an international river basin* (1st ed., pp. 251–272). https://doi.org/10.1016/B978-0-12-374026-7.00010-3

European Space Agency. (2017). *Land Cover Product* (Phase 2 Global Land Cover Maps) [Data set]. Climate Change Institute. https://maps.elie.ucl.ac.be/CCI/viewer/

Göttl, F., Dettmering, D., Müller, F. L., & Schwatke, C. (2016). Lake level estimation based on CryoSat-2 SAR altimetry and multi-looked waveform classification. *Remote Sensing*, *8*(11), 1–16. https://doi.org/10.3390/rs8110885

Hossain, F., Sikder, S., Biswas, N., Bonnema, M., Lee, H., Luong, N. D., … Long, D. (2017). Predicting Water Availability of the Regulated Mekong River Basin Using Satellite Observations and a Physical Model. *Asian Journal of Water, Environment and Pollution*, *14*(3), 39–48. https://doi.org/10.3233/AJW-170024

Lin, Z., & Qi, J. (2017). Hydro-dam – A nature-based solution or an ecological problem: The fate of the Tonlé Sap Lake. *Environmental Research*, *158*, 24–32. https://doi.org/https://doi.org/10.1016/j.envres.2017.05.016

Mahood, S. P., Poole, C. M., Watson, J. E. M., MacKenzie, R. A., Sharma, S., & Garnett, S. T. (2020). Agricultural intensification is causing rapid habitat change in the Tonle Sap Floodplain, Cambodia. *Wetlands Ecology and Management*, *28*(5), 713–726. https://doi.org/10.1007/s11273-020-09740-1

Ministry of Environment. (2018). *Cambodia Land Use / Land Cover* (2016 Update) [Data set]. Kingdom of Cambodia https://redd.unfccc.int/uploads/54_3_cambodia_forest_cover_resource__2016_english.pdf

Nuorteva, P., Keskinen, M., & Varis, O. (2010). Water, livelihoods and climate change adaptation in the Tonle Sap lake area, Cambodia: Learning from the past to understand the future. *Journal of Water and Climate Change*, *1*(1), 87–101. https://doi.org/10.2166/wcc.2010.010

Pettorelli, N., Safi, K., & Turner, W. (2014). Satellite remote sensing, biodiversity research and conservation of the future. *Philosophical Transactions of the Royal Society B: Biological Sciences*, *369*(1643). https://doi.org/10.1098/rstb.2013.0190

Ross, M. R. V., Topp, S. N., Appling, A. P., Yang, X., Kuhn, C., Butman, D., … Pavelsky, T. M. (2019). AquaSat: A data set to enable remote sensing of water quality for inland waters. *Water Resources Research*, *55*(11), 10012–10025. https://doi.org/10.1029/2019WR024883

Saah, D., Johnson, G., Ashmall, B., Tondapu, G., Tenneson, K., Patterson, M., … Chishtie, F. (2019). Collect Earth: An online tool for systematic reference data collection in land cover and use applications. *Environmental Modelling and Software*, *118*(March), 166–171. https://doi.org/10.1016/j.envsoft.2019.05.004

Saah, D., Tenneson, K., Matin, M., Uddin, K., Cutter, P., Poortinga, A., … Chishtie, F. (2019). Land cover mapping in data scarce environments: Challenges and opportunities. *Frontiers in Environmental Science*, *7*(November). https://doi.org/10.3389/fenvs.2019.00150

Schüßler, D., Mantilla-Contreras, J., Stadtmann, R., Ratsimbazafy, J. H., & Radespiel, U. (2020). Identification of crucial stepping stone habitats for biodiversity conservation in northeastern Madagascar using remote sensing and comparative predictive modeling. *Biodiversity and Conservation*, *29*(7), 2161–2184. https://doi.org/10.1007/s10531-020-01965-z

Schwatke, C., Scherer, D., & Dettmering, D. (2019). Automated extraction of consistent time-variable water surfaces of lakes and reservoirs based on Landsat and Sentinel-2. *Remote Sensing, 11*(9), 1010. https://doi.org/10.3390/rs11091010

Schwatke C., Dettmering D., Bosch W., & Seitz F. (2015). *DAHITI, Database for Hydrological Time Series of Inland Waters* (Water Level Time Series from Satellite Altimetry) [Data set]. Deutsches Geodätisches Forschungsinstitut der Technischen Universität München. https://doi.org/10.5194/hess-19-4345-2015

SERVIR Mekong (2020). *Regional Land Cover Monitoring System* (Lower Mekong Basin) [Class Primitives]. Bangkok, Thailand. https://www.landcovermapping.org/en/landcover/

Spruce, J., Bolten, J., Srinivasan, R., & Lakshmi, V. (2018). Developing land use land cover maps for the lower mekong basin to aid hydrologic modeling and basin planning. *Remote Sensing*, *10*(1910), 1–26. https://doi.org/10.3390/rs10121910

Uk, S., Yoshimura, C., Siev, S., Try, S., Yang, H., Oeurng, C., … Hul, S. (2018). Tonle Sap Lake: Current status and important research directions for environmental management. *Lakes & Reservoirs*, *23*(3), 177–189. https://doi.org/10.1111/lre.12222

Vollmer, D., Shaad, K., Souter, N. J., Farrell, T., Dudgeon, D., Sullivan, C. A., … Regan, H. M. (2018). Integrating the social, hydrological and ecological dimensions of freshwater health: The Freshwater Health Index. *Science of the Total Environment*, *627*, 304–313. https://doi.org/10.1016/j.scitotenv.2018.01.040

Wang, Y., Feng, L., Liu, J., Hou, X., & Chen, D. (2020). Changes of inundation area and water turbidity of Tonle Sap Lake: Responses to climate changes or upstream dam construction? *Environmental Research Letters*, *15*(9). https://doi.org/10.1088/1748-9326/abac79

9. Appendices

Appendix A. Altimetry

Table A1. Satellite Altimeters used in DAHITI (Source: Schwatke et al. 2015)

Mission	Product	Source	Cycle Length	Date Range
Envisat	SGDR (v2.1)	ESA	35 d	2002-2010
Envisat (EM)	SGCR (v2.1)	ESA	35 d	2010-2011
ERS-21	SGDR (REAPER)	ESA	35 d	1995-2007
Jason-1	SGDR-C	ESA, NASA	9.9156 d	2002-2009
Jason-1 (EM)	SGDR-C	ESA, NASA	9.9156 d	2009-2012
Jason-1 (GM)	SGDR-C	ESA, NASA	9.9156 d	2012-2013
Jason-2	SGDR-D	ESA, NASA	9.9156 d	2008-active

Poseidon	ALT SDR (L1B)	ESA, NASA	9.9156 d	1992-2002
TOPEX	ALT SDR (L1B)	ESA, NASA	9.9156 d	2002-2005
SARAL/ AltiKa		NASA, EUMETSAT	25 d	2013-active

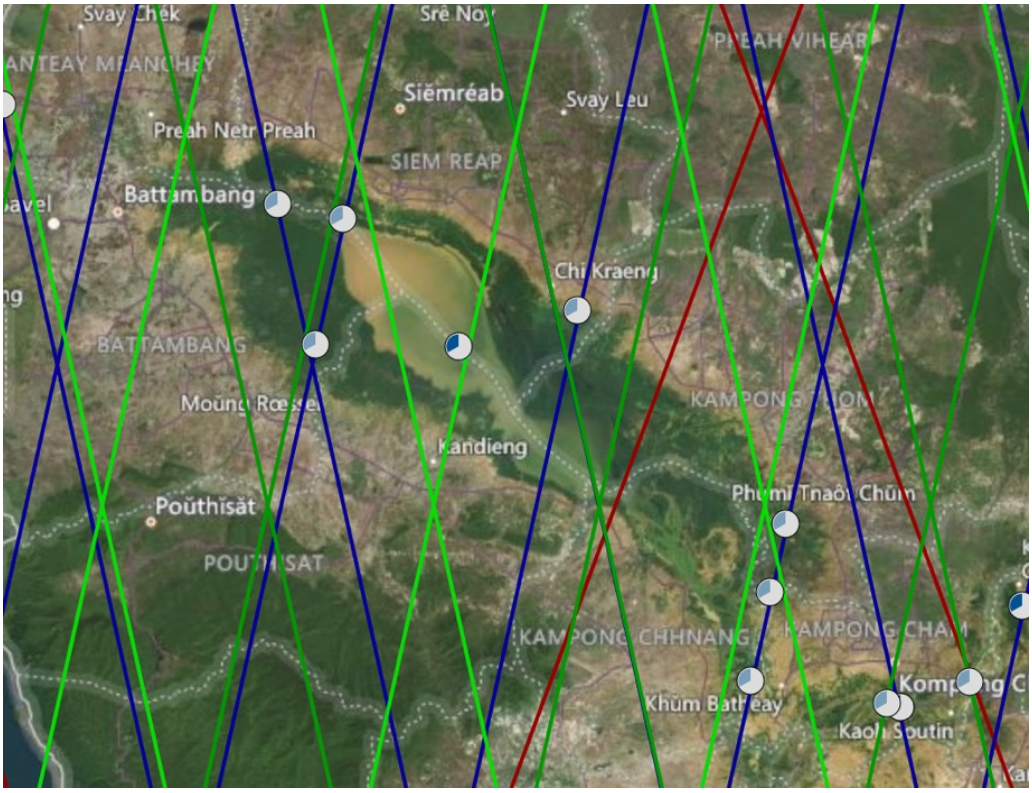

Figure A1. Altimetry Satellite tracks across Tonlé Sap, along with nodes for which DAHITI aggregates altimetry data. Dark blue: Envisat; Dark red: Jason2; Dark green: Sentinel-3A; Light green: Sentinel-3B).

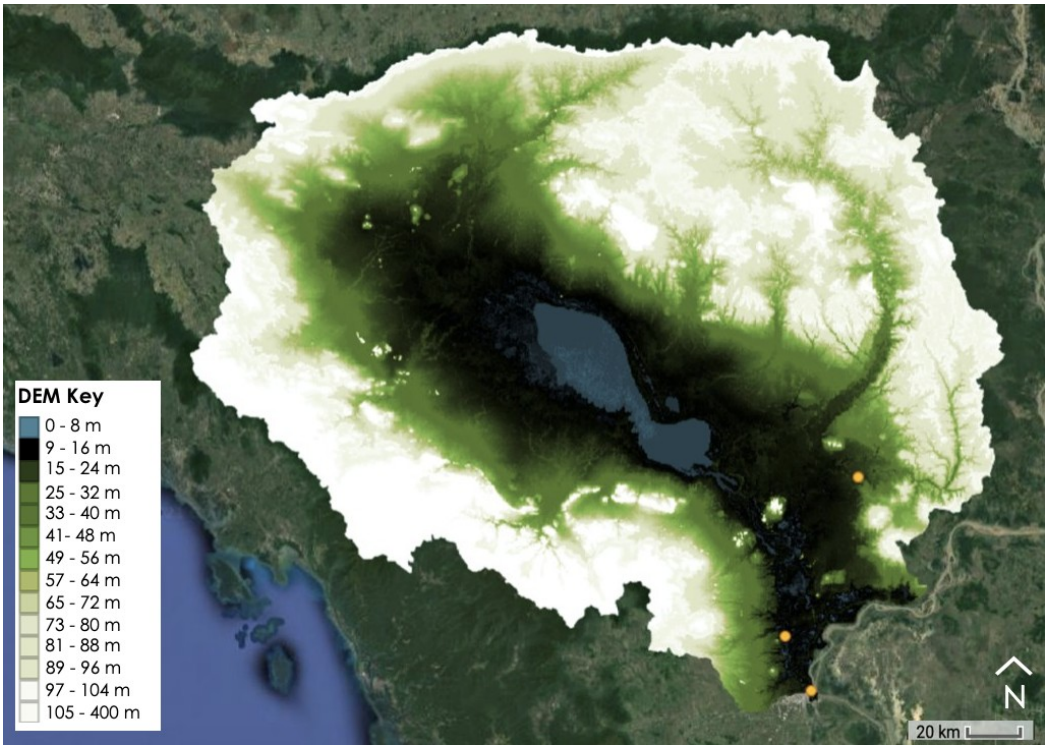

Figure A2. Map of *in situ* river gauge locations (orange) on top of HydroSHEDS DEM. River gauges are indicated by yellow markers in the southeast region of the image.

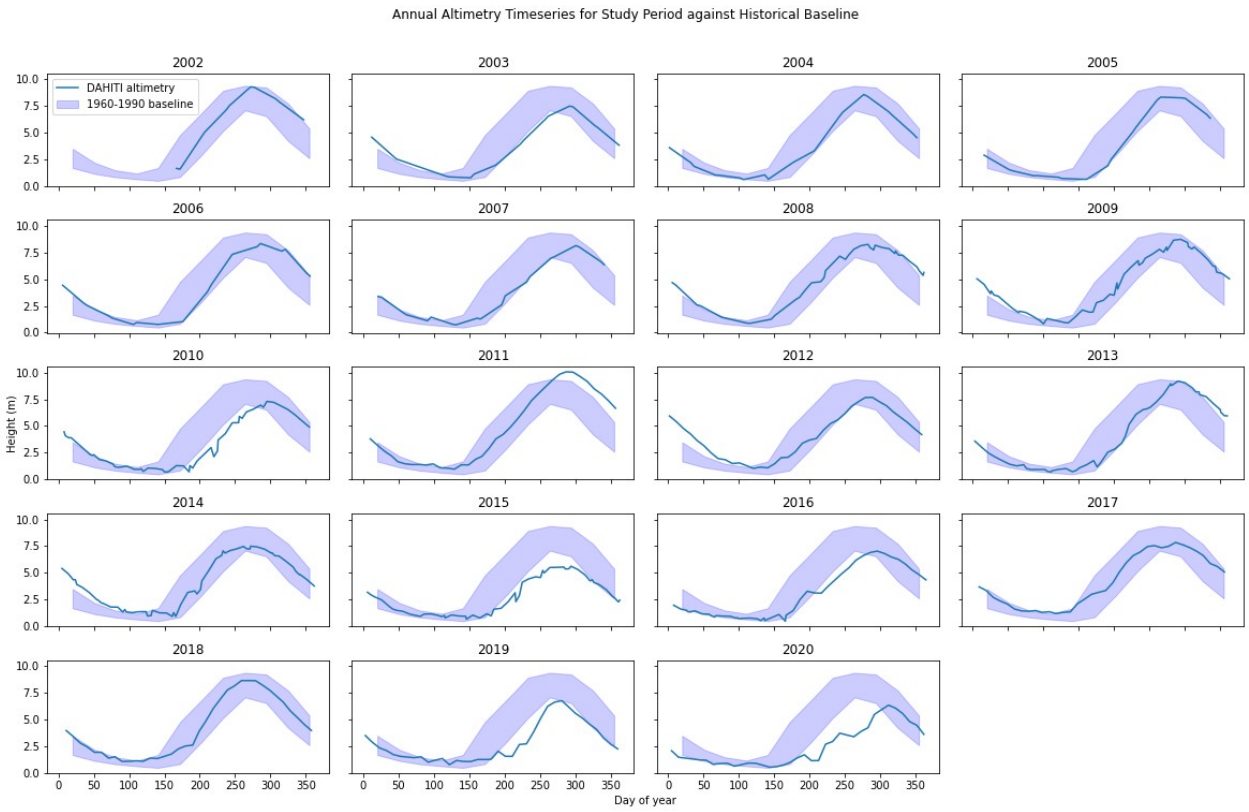

Figure A3. Annual altimetry data for each year of the study period plotted against the historical monthly averages, -/+ 1 standard deviations.

Appendix B. Land Cover Naturalness and Bank Modification

Table B1. Landcover Classification Inputs

Dataset	Product Used	Classification Created
CGLS-LC100 Collection 3	Landcover map	Baseline Naturalness (globally applicable) classification
CCI Landcover	Landcover map	Baseline Naturalness (globally applicable) classification
FAO Cambodia Ministry of Energy Dataset	Landcover map	Government-Compatible classification
SERVIR Mekong RLCMS	Landcover map and class primitives	FHI-Oriented classification, Rice harvest frequency map, Forest change detection
NASA Shuttle Radar Topography Mission Digital Elevation Model (STRM DEM)	Digital elevation model	FHI-Oriented classification, Rice harvest frequency classification
Terra Moderate Resolution Imaging Spectroradiometer (MODIS)	Normalized Difference Vegetation Index, Normalized Difference Water Index, Land surface temperature	FHI-Oriented classification, Rice harvest frequency classification
Aqua Moderate Resolution Imaging Spectroradiometer (MODIS)	Normalized Difference Vegetation Index, Normalized Difference Water Index, Land surface temperature	FHI-Oriented classification, Rice harvest frequency classification
Visible Infrared Imaging Radiometer Suite (VIIRS)	Normalized Difference Vegetation Index	FHI-Oriented classification, Rice harvest frequency classification
Landsat 8 OLI	Normalized Difference Vegetation Index, Normalized Difference Water Index	FHI-Oriented classification, Rice harvest frequency classification

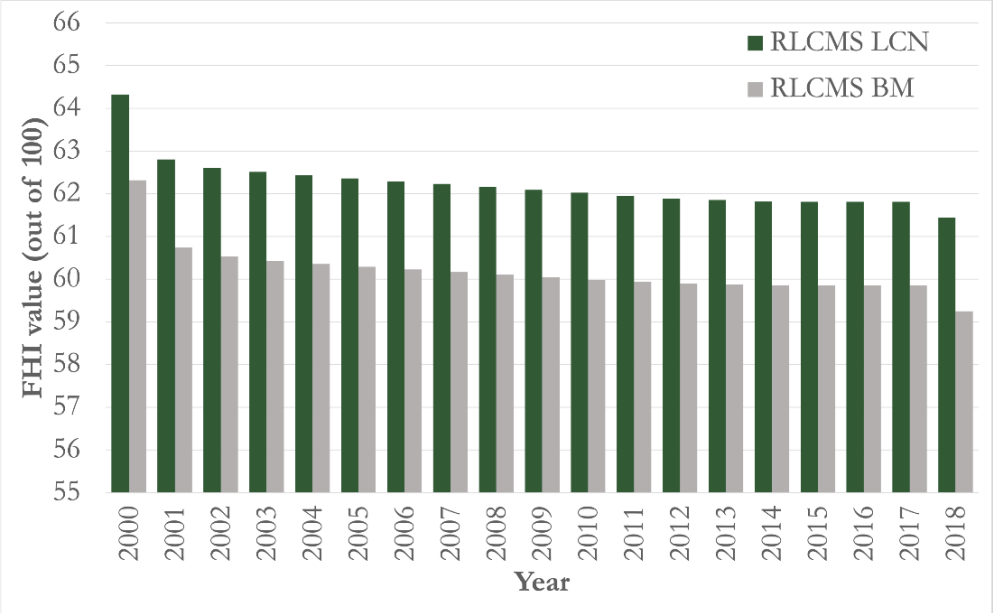

Figure B2. Land Cover Naturalness (LCN) and Bank Modification (BM) graphed for SERVIR RLCMS landcover dataset.

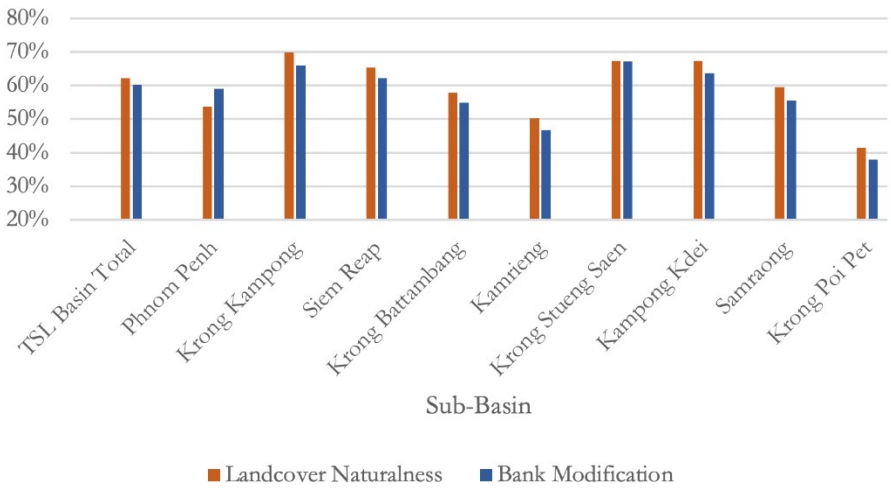

Figure B3. LCN and BM outputs based on SERVIR data, segmented by sub-basin and averaged across all years.

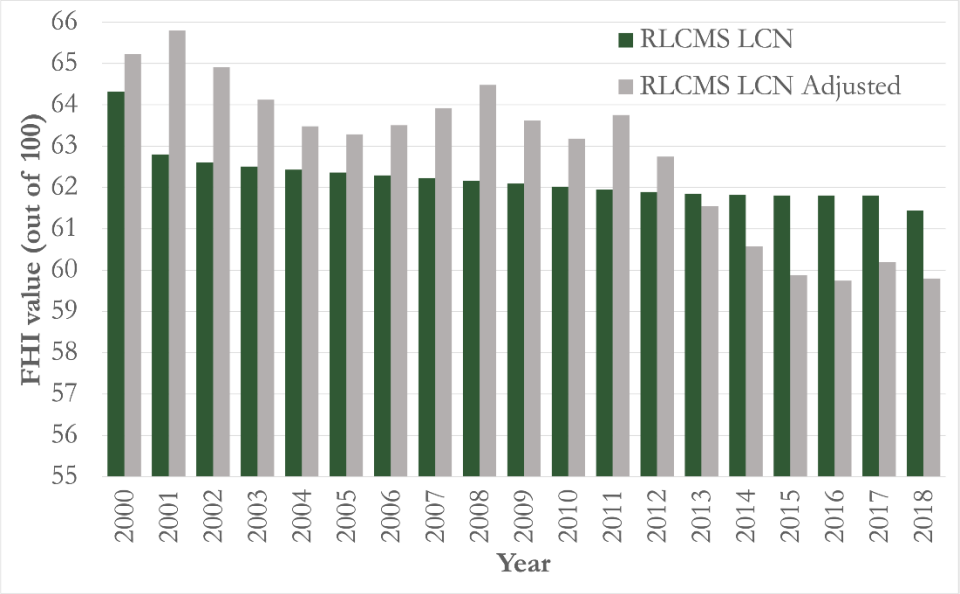

Figure B4. LCN graphed for SERVIR RLCMS before and after proportional adjustment based on accuracy.

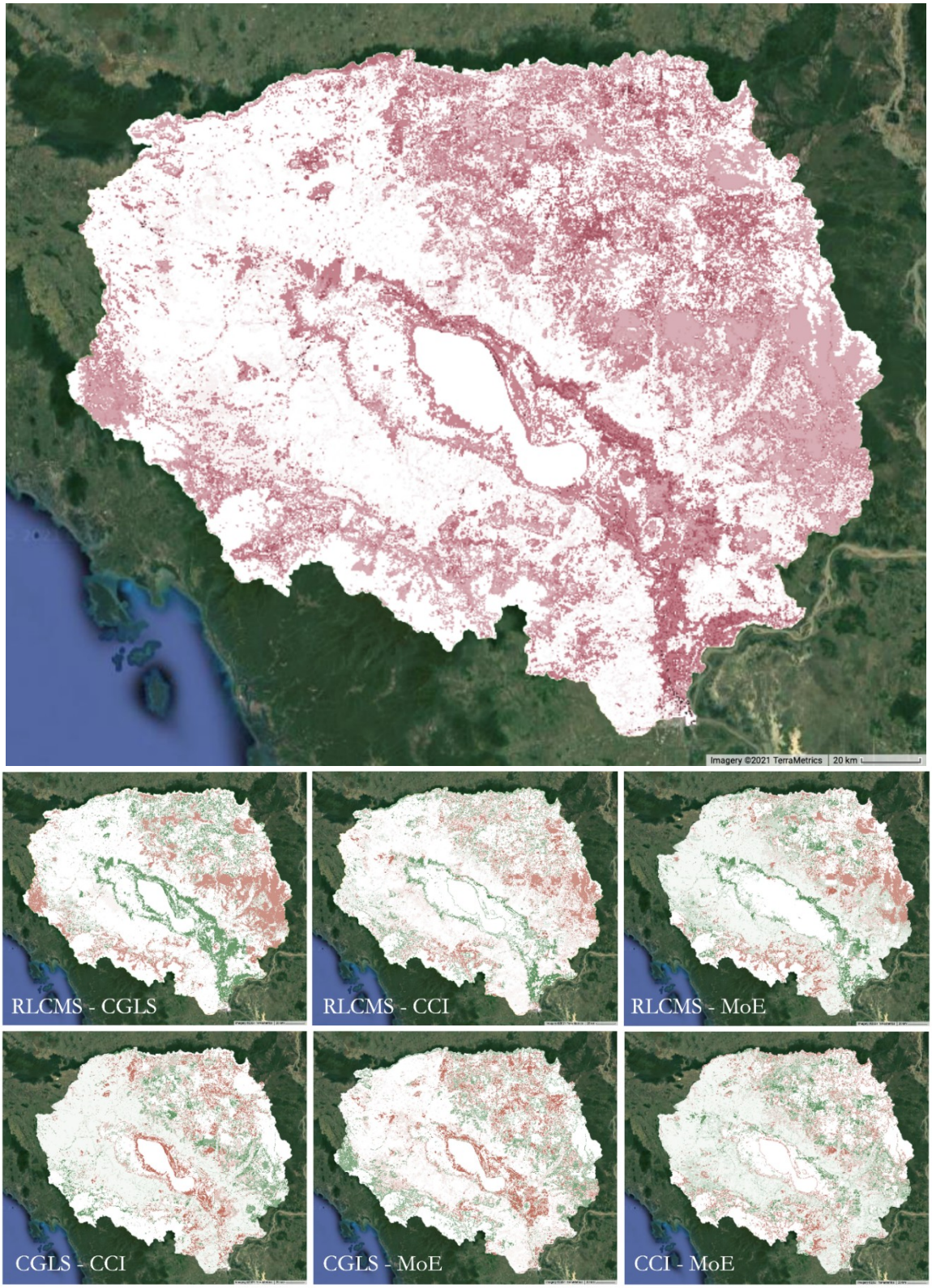

Figure B5. Variance map comparing naturalness score determinations (changes visualized in red); difference maps comparing each pair of classifications for 2015 (and 2016 for MoE) (divergent changes visualized in red and green).

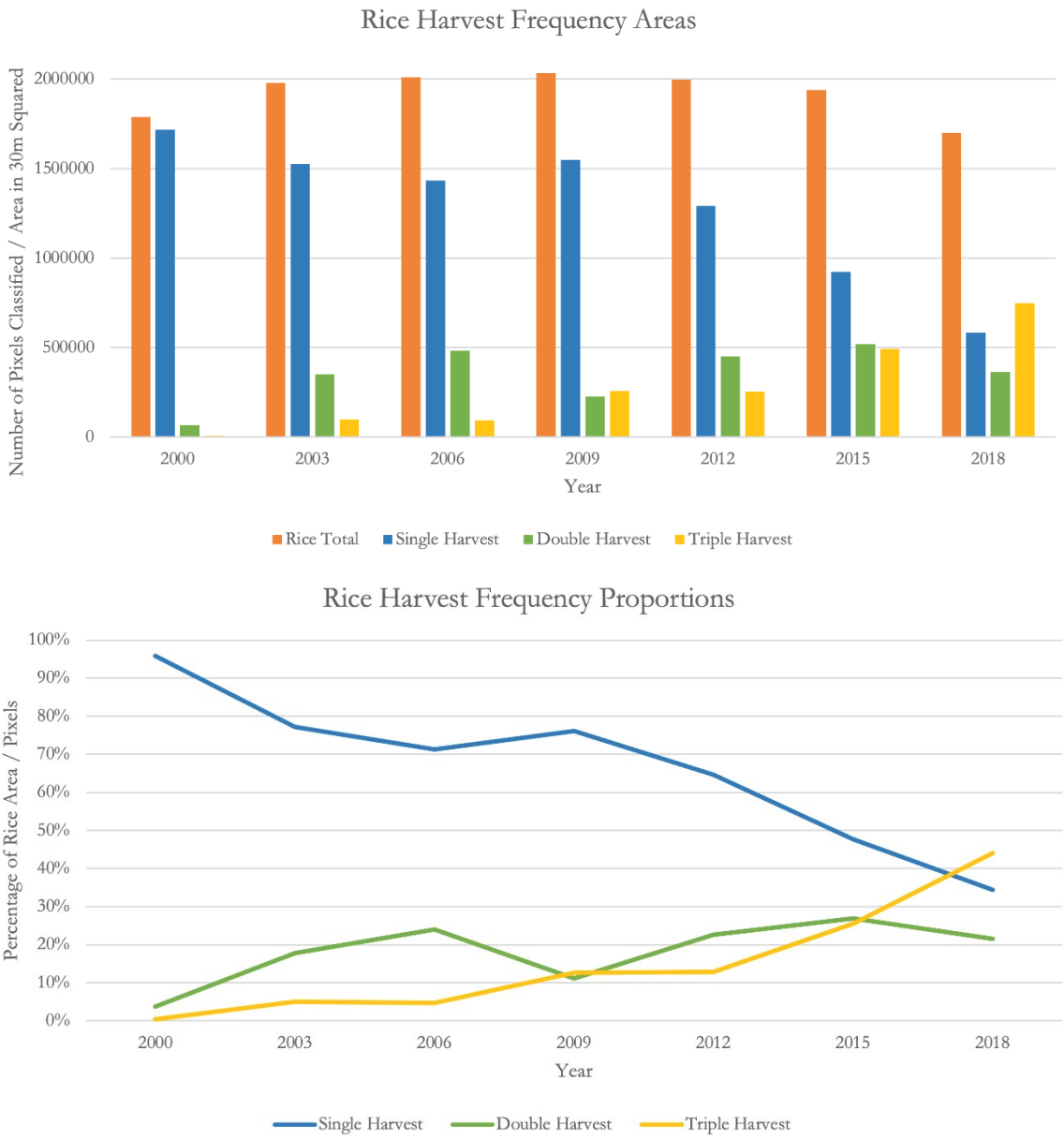

Figure B6. Rice Harvest Frequency Graphs